Quantifying the complexity of bat wing kinematics

Daniel K. Riskin[1,†], David J. Willis[2], Jose Iriarte-Diaz[1], Tyson L. Hedrick[3], Mykhaylo Kostandov[4], Jian Chen[4], David H. Laidlaw[4], Kenneth S. Breuer[5], and Sharon M. Swartz[1,5]

[1]*Department of Ecology and Evolutionary Biology, Brown University, Providence, RI 02912 USA*

[2]*Department of Aeronautics and Astronautics, Massachusetts Institute of Technology, Cambridge MA 02139 USA*

[3]*Department of Biology, CB 3280 Coker Hall, University of North Carolina, Chapel Hill, NC 27599 USA*

[4]*Department of Computer Science, Brown University, Providence, RI 02912 USA*

[5]*Division of Engineering, Brown University, Providence, RI 02912 USA*

[†]Author for correspondence:

Daniel K. Riskin (dkr8@brown.edu)

Department of Ecology and Evolutionary Biology, Brown University

171 Meeting St., #204

Providence, RI 02912, USA

Tel: 617-894-9998

ABSTRACT

Body motions (kinematics) of animals can be dimensionally complex, especially when flexible parts of the body interact with a surrounding fluid. In these systems, tracking motion completely can be difficult, and result in a large number of correlated measurements, with unclear contributions of each parameter to performance. Workers typically get around this by deciding *a priori* which variables are important (wing camber, stroke amplitude, etc.), and focusing only on those variables, but this constrains the ability of a study to uncover variables of influence.

Here, we describe an application of Proper Orthogonal Decomposition for assigning importances to kinematic variables, using dimensional complexity as a metric. We apply this method to bat flight kinematics, addressing three questions: (1) Does dimensional complexity of motion change with speed? (2) What body markers are optimal for capturing dimensional complexity? (3) What variables should a simplified reconstruction of bat flight include in order to maximally reconstruct actual dimensional complexity?

We measured the motions of 17 kinematic markers (20 joint angles) on a bat (*Cynopterus brachyotis*) flying in a wind tunnel at nine speeds. Dimensional complexity did not change with flight speed, despite changes in the kinematics themselves, suggesting that the relative efficacy of a given number of dimensions for reconstructing kinematics is conserved across speeds.

By looking at subsets of the full 17-marker set, we found that using more markers improved resolution of kinematic complexity, but that the benefit of adding markers

Daniel K. Riskin 5/8/08 9:59 AM
Deleted: complexity

diminished as the total number of markers increased. Dimensional complexity was highest when the hindlimb and several points along digits III and IV were tracked.

Also, we uncovered three groups of joints that move together during flight by using POD to quantify correlations of motion. These groups describe 14/20 joint angles, and provide a framework for models of bat flight for experimental and modeling purposes.

KEYWORDS Proper Orthogonal Decomposition, Kinematic Markers, Joint Angles

1. Introduction

1.1 Complexity of bat flight

In flight, a bat performs rapid three-dimensional folding, bending, and rotational wing movements to generate aerodynamic force, thereby imparting a highly structured wake pattern to the air behind it (Hedenström *et al.*, 2007; Muijres *et al.*, 2008; Tian *et al.*, 2006). Models of this system, be they focused on neuromuscular control, aerodynamic function, or energetics, can only be as accurate as the kinematic reconstructions upon which they are based. One way to develop simplified but accurate models may be through investigation of dimensional complexity. For instance, if different parts of the wing move together as functional units, identification of those units can motivate improved simplified models. Similarly, by measuring complexity we can say whether such models might be more applicable at certain speeds, where complexity is lower. Furthermore, we can quantify the efficacy of different sets of kinematic markers for accurately tracking bat flight kinematics. In this paper, we apply Proper Orthogonal Decomposition (POD), a computational tool, to the wing kinematics of a bat flying in a wind tunnel, with the purpose of quantifying the dimensional complexity of movement during steady flight over a range of speeds.

For the purposes of this paper, we define dimensional complexity as linear multidimensionality of motion among moving parts of a body. If all the parts of the body move together in such a way that the position of any body part can be calculated from a simple linear equation based on the position of any other, dimensional complexity is low. If, however, the parts of a body move independently, description of a body's posture requires the tracking of many more variables. In that case, dimensional complexity of

Daniel K. Riskin 5/7/08 12:48 PM
Deleted: movement

Daniel K. Riskin 5/7/08 12:48 PM
Deleted: a

Daniel K. Riskin 5/7/08 11:19 AM
Deleted: known

Daniel K. Riskin 5/7/08 11:19 AM
Deleted: from

movement, by our definition, is high. Because we use POD, our analyses are sensitive to changes in the linear relationships among moving body parts. There are several other ways in which complexity might change that are not sensitive to our analyses (Tresch *et al.*, 2006). However, POD is used quite widely in analyses of gait and other biological movements (Cappellini *et al.*, 2006; Chau, 2001; Forner-Cordero *et al.*, 2007; Ivanenko *et al.*, 2008; Mason *et al.*, 2001; Todorov & Ghahramani, 2004; Tripp *et al.*, 2006), so we expected POD to reveal useful information about kinematic complexity in this application as well.

Bat flight has the potential to be extremely dimensionally complex. A bat wing membrane is maneuvered skeletally by a jointed leg, a shoulder, an elbow, a wrist, and by five fingers, each with several joints. Adding up joints alone, this provides >20 degrees of kinematic freedom per wing. Additionally, movement is influenced by the flexibility of the bony elements within the wing, the orientation-dependent compliance of the membranes, their interactions with the surrounding fluid, and by movements of the numerous tendons and muscles within the membranes themselves (Norberg, 1972; Swartz *et al.*, 1992; Swartz *et al.*, 1996).

It is clear from a broad range of studies that bats move their limbs in complicated ways during locomotion (Aldridge, 1986; Aldridge, 1987a; Aldridge, 1987b; Hedenström *et al.*, 2007; Lindhe Norberg & Winter, 2006; Norberg, 1969; Norberg, 1976a; Norberg, 1976b; Rayner & Aldridge, 1985; Riskin *et al.*, 2005; Riskin & Hermanson, 2005; Riskin *et al.*, 2006; Tian *et al.*, 2006; Watts *et al.*, 2001). However, despite the potential for high dimensional complexity, there are at least three reasons we expect movements at several joint angles in a flying bat to be closely correlated. First, it is common in animals for

multiple joints to be activated together by a common signal from the nervous system, or for a single muscle to actuate more than one joint (Goslow, 1985). Second, the aerodynamics of flapping flight presumably require that parts of the wing move together in a coordinated fashion so that an organized wake structure can be shed behind the wing (Hedenström *et al.*, 2007; Rosen *et al.*, 2004; Spedding, 1987; Spedding *et al.*, 1984; Spedding *et al.*, 2003; Tian *et al.*, 2006). Third, different parts of the wing should move together because they are physically connected in a way that presumably prevents independence of motion. Therefore, although the number of degrees of freedom of motion possible for a bat skeleton is high, the actual dimensional complexity of motion might be low.

Daniel K. Riskin 5/7/08 1:11 PM
Deleted: might be

Several authors, most notably Aldridge and Lindhe Norberg, have reported bat flight kinematics in great detail (Aldridge, 1986; Aldridge, 1987a; Aldridge, 1987b; Lindhe Norberg *et al.*, 2000; Lindhe Norberg & Winter, 2006; Norberg, 1969; Norberg, 1970; Norberg, 1976a; Norberg, 1976b). Their studies demonstrate that wing kinematics change predictably with speed, but do not quantify the complexity of motion. If the dimensional complexity of bat flight changes with speed, the number of markers required to accurately record bat flight kinematics may be velocity-dependent. Also, researchers seeking to model bat flight could focus their preliminary efforts on velocity regimes where complexity is low. POD permits us to address the influence of speed on dimensional complexity of kinematics, and to test the efficacies of different numbers of kinematic markers for reconstructing body kinematics.

Daniel K. Riskin 5/7/08 1:11 PM
Deleted: kinematic

1.2 Proper Orthogonal Decomposition

Proper Orthogonal Decomposition is a ca. 100-year old computational tool (Hotelling, 1933; Pearson, 1901) that has recently been applied to the analysis of organismal kinematics (Chatterjee, 2000; Feeny & Kappagantu, 1998; Tangorra *et al.*, 2007). Proper Orthogonal Decomposition is mathematically equivalent to principal components analysis (Daffertshofer *et al.*, 2004), with the difference in terminology arising from adoption of the same technique by different branches of the sciences and POD more often referring to application of the technique to a dynamical system. In POD, the user places the three-dimensional positions of m markers over time into an N x $(3 \cdot m)$ matrix **A** such that each column describes the time-dependent displacement history of a marker in one dimension: $\mathbf{a}_i = (a_i(t_1), a_i(t_2), \ldots, a_i(t_N))^T$, for $i = 1, \ldots, (3 \cdot m)$. Each row of the resulting matrix completely describes the concurrent three-dimensional marker positions at some instant in time. The $(3 \cdot m)$ x $(3 \cdot m)$ correlation matrix $\mathbf{R} = (1/N)\mathbf{A}^T\mathbf{A}$ is then formed, and its eigenvectors form an orthogonal basis. These eigenvectors are called proper orthogonal modes, and the percentage of the overall motion described by each mode is defined by its associated normalized eigenvalue (Feeny & Kappagantu, 1998).

The modes of **R** have the characteristic that the first (mode 1, or ξ_1) describes the greatest possible proportion of the movement of any possible vector in the subspace. The second mode (ξ_2) is orthogonal to ξ_1, and describes the greatest possible proportion of the movement that remains, and so on. As the number of modes increases, the reconstructed movement described by the sum of k modes ($\xi_1 + \xi_2 + \ldots + \xi_k$) converges more and more closely to the original movement, and the sum of all modes ($k = 3 \cdot m$) reproduces the movement completely (Liang *et al.*, 2002).

1.3 Goals of the study

In the first part of this study, we examined whether the complexity of bat movement changes with speed by looking at the number of POD modes required to closely reproduce the original movement. By our definition, a motion that has high dimensional complexity requires more modes to be reproduced accurately than a motion that has low dimensional complexity.

In the second part, we used POD to quantify the relative dimensional complexities captured by using different numbers of anatomical markers in studies of bat kinematics. When too few markers are used, the motion will appear less complex than it actually is, while we expect an overabundance of markers to be kinematically redundant, and unnecessarily increase the amount of time required to digitize kinematics. We used POD to ask how many, and which, marker locations are optimal to most closely approximate the actual dimensional complexity of wing kinematics. We predicted that the dimensional complexity of a marker set would increase as the number of markers in that set increased, but that this would be an asymptotic change, and that after some number of markers there would be relatively little increase in the complexity of motion captured by adding more markers. We also expected that complexity should differ for a given number of markers, depending where those markers were placed. If all markers were placed on a single bone, for example, dimensional complexity, as defined here, would be low. Markers distributed among body parts that move independently would have comparatively higher $\xi_{95\%}$ values, and lower P_{ξ_i} values. Our methods, then, might elucidate redundancies among marker sets. Our hope was that these results might inform selection of the number and position of anatomical markers in future studies of bat kinematics.

Daniel K. Riskin 5/10/08 1:01 PM
Formatted: Font:Not Italic, Not Superscript/ Subscript

In the third part of the study we used POD to assess the similarity of motion of joint angles throughout the skeleton to find functional groups of joints that are actuated in synchrony by the flying bat. We predicted that joints moving in synchrony should be located close together on the wing because units controlled together for aerodynamic purposes would likely appear close together, and because units controlled by a common part of the neuromuscular control hierarchy should presumably be nearby one another. Because this form of analysis is numerical, it makes no assumptions about aerodynamic or morphological control, aerodynamic function, or mechanics, making it particularly useful where *a priori* assumptions about the relative importance of different joints are to be avoided.

2. Methods

2.1 Video recording of the bat

Because POD results are affected by differences in relative marker positions (Daffertshofer *et al.*, 2004), we eliminated morphological variability by using the flights of a single adult female Lesser Dog-faced Fruit Bat (Pteropodidae: *Cynopterus brachyotis*) over a range of flight speeds. All components of this study were approved by the Institutional Animal Care and Use Committees at Brown University, Harvard University, and the Lubee Bat Conservancy, and by the United States Air Force Office of the Surgeon General's Division of Biomedical Research and Regulatory Compliance.

The bat was anesthetized with isofluorane gas, and a series of markers was placed on the fur and skin. On fur, we used non-toxic acrylic paint, and on the wing membrane we used small pieces of reflective tape. We only tracked markers on one the left half of

the body. The marked bat was flown in a wind tunnel (Harvard University Concord Field Station Wind Tunnel, test section: 1.4 m length, 1.2 m width, 1.2 m height) in nine consecutive trials. The characteristics of this wind tunnel were described in detail by Hedrick et al. (Hedrick *et al.*, 2002). We recorded the flying bat at 1000 Hz using three phase-locked Photron 1024 PCI digital high-speed cameras (Photron USA, Inc., San Diego CA, USA).

The volume of the wind tunnel in which the bat was flown was calibrated using the Direct Linear Transformation method, based on a 40-point calibration cube (Hedrick *et al.*, 2004). From each video frame, the positions of 17 anatomical markers were digitized (Figure 1), and their positions in three-dimensional space calculated with a custom-built program in MATLAB (MathWorks, Inc., Natick MA, USA). We estimated the accuracy of our position measurements by examining the distribution of distances between the two sternum markers (mean 2.23 cm) over all trials, and found standard deviation 0.05 cm (standard error less than 3%), with maxima and minima differing by <0.5 cm.

In each trial, we captured the largest possible integer number of consecutive wingbeats while the bat flew in a fixed position within the calibrated volume. We used the vertical position of the wrist marker to delineate the endpoints of each wingbeat cycle. This resulted in nine separate trials, one consisting of two wingbeats, six of three wingbeats, and two of four wingbeats. The velocity of the bat's anterior sternum marker (*a* in Figure 1) was added to air speed to arrive at net velocity for each trial. To be sure that the flight of the single individual used in this experiment was representative of the species, wing movements from six other adult female *C. brachyotis* were recorded in the

same way over 42 trials. Their wingbeat frequencies, amplitudes, and flight speeds were similar to those of the bat used in this study, but are not presented here.

2.2 Post-processing of kinematic data

We used videos to reconstruct the positions of 17 markers at 4,222 different points in time, or 71,774 marker-moments. At those moments where a marker was not visible to at least two cameras, its position could not be calculated. This occurred in 11,180 (15.6%) of marker-moments. We filled these gaps in the kinematic data with a custom curve-fitting algorithm based on over-constrained least-squares polynomial fitting. For contiguous gaps in the data, with sufficiently rich data at the end points, a third order, over-constrained polynomial fit was used. For gaps that included sporadic intermediate points, a sixth order polynomial was used. After gap-filling, we used a 50 Hz lowpass Butterworth filter to remove high-frequency noise. This cutoff frequency was around 4.5 times higher than the highest wingbeat frequency we recorded (10.4 Hz).

Three-dimensional coordinates of each marker were transformed to a body-referenced linear coordinate system, with the anterior sternum (*a* in Figure 1) at [0, 0, 0]. The *x*-axis was a line through the two sternum markers (positive = toward anterior), the *y*-axis was orthogonal to the *x*-axis and gravity (positive = left of flight direction, toward wingtip), and the *z*-axis was orthogonal to *x* and *y* (positive = dorsal). From the motions of the markers, we also calculated 20 separate joint angles (Table 1).

2.3 Proper Orthogonal Decomposition

For POD of the marker positions (Parts 2.4 and 2.5, below), the three-dimensional coordinates of each of the 17 markers through the trial were placed in a matrix. The x, y, and z coordinates of the anterior sternum marker and the y and z values of the posterior sternum marker remained at zero at all times by definition, and were therefore omitted. As a result, the size of the matrix, using 17 markers, was $t \times 46$, where t is the length of the trial, in milliseconds. We subtracted the mean values for each column from all values in that column, and performed POD using singular value decomposition of the transposed matrix in MATLAB (Chatterjee, 2000). For POD of joint angles (parts 2.4 and 2.6, below), we repeated this procedure for the $t \times 20$ matrix of joint angles.

In studies that employ POD, researchers frequently normalize, by dividing each value by the standard deviation of its column before POD, so that variables are not weighted by absolute magnitude; the wingtips in our study, for example, would not be weighted more heavily than anatomical locations that move shorter distances (Daffertshofer *et al.*, 2004). This is numerically equivalent to using the correlation matrix in Principal Components Analysis. However, points moving through larger distances might well be more 'important,' depending on the objective of the research, so normalizing the variance of all markers might remove relevant information. Alternatively, the relative amplitudes of motion could be weighted to keep signal-to-noise ratios constant, or in any other arbitrarily chosen manner. In this study, we chose to standardize variance before performing POD. We thought it appropriate to standardize variance for POD of joint angles, since the complexity of control should not change linearly with amplitude of motion, and decided to use the same methods for joint angles and marker positions, for ease of comparison.

259

260 *2.4: Measuring changes in dimensional complexity with flight speed*

261 When the percentage of original motion captured by cumulative POD modes is
262 plotted against the number of modes used, the curve asymptotically approaches 100%,
263 until the motion is completely described when all modes are included. As a summary
264 statistic of that curve for each POD analysis, we used the number of modes required to
265 describe 95% of the movement, $\xi_{95\%}$. To calculate this, we made a spline fit through the
266 aforementioned curve, and defined $\xi_{95\%}$ as the x-axis value where that function crossed
267 95%; by our definition, higher $\xi_{95\%}$ values indicate greater dimensional complexity. To
268 determine whether the kinematic complexity of wing motions changed with speed, we
269 carried out linear regressions of $\xi_{95\%}$ versus speed. This was done twice, once for the
270 motion of points and once for the motions of joint angles.

271 Because no two wingbeats were kinematically identical, it is possible that the
272 number of wingbeats could influence the kinematic complexity of a trial. If so, trials with
273 fewer wingbeats would have lower $\xi_{95\%}$ *values* than trials with more wingbeats. We
274 looked for this trend in our data, to verify that treating all trials equally, regardless of
275 number of wingbeats, was justified.

276

277 *2.5: Testing the efficacies of kinematic marker positions*

278 We used POD to quantify the relative complexities of motion revealed by varying
279 numbers and positions of wing markers. To assess complexity, we performed POD on
280 every possible combination of markers, from the two sternum markers alone to the
281 complete 17. This required $2^{15} = 32{,}768$ separate POD analyses per trial. For each

number of markers, we sought the set that captured the highest degree of dimensional complexity. We were unable to use $\xi_{95\%}$ however, since for small numbers of markers, the $\xi_{95\%}$ value is difficult to calculate due to the small number of points through which a spline is to be interpolated. Instead, we used a value we call $P_{\xi 1}$: the percentage of original motion captured by the first POD mode. Sets of markers that move independently of one another should be characterized by a relatively lower $P_{\xi 1}$ value. We used the mean $P_{\xi 1}$ value for each marker set across the nine trials as an index of dimensional complexity for that marker set.

2.6: Finding groups of joint angles that move together

We used POD to quantify the similarity of motion for all 190 pairs of joints (20 choose 2 = 190). For each pair, POD was performed on the t × 2 matrix of joint angles, and $P_{\xi 1}$ was calculated. A cluster tree was then constructed using the average linkage function in Matlab. The average linkage function uses the unweighted average distance between all pairs of objects in cluster *r* and cluster *s* according to the formula

$$d(r,s) = \frac{1}{n_r n_s} \cdot \sum_{i=1}^{n_r} \sum_{j=1}^{n_s} dist(x_{ri}, x_{sj}),$$

where n_r is the number of joint angles in cluster *r*, n_s is the number of joint angles in cluster *s*, x_{ri} is the i^{th} object in cluster *r*, x_{sj} is the j^{th} object in cluster *s*, and *dist* is defined as $(1-P_{\xi 1})$. The result was a dendrogram of joint angles that clustered joint angles based on similarity of motion.

3. Results

Daniel K. Riskin 5/10/08 11:59 AM
Deleted: divided by the number of degrees of freedom that went into that POD analysis (e.g. 3 for 1 wing marker, to 45 for 15 wing markers)

Daniel K. Riskin 5/10/08 12:00 PM
Deleted: ,

Daniel K. Riskin 5/7/08 1:38 PM
Deleted: that uses the average distance between all pairs of objects in each cluster, using (1- $P_{\xi 1}$) values to form the dissimilarity matrix.

Daniel K. Riskin 5/7/08 3:01 PM
Formatted: Indent: First line: 0"

Daniel K. Riskin 5/7/08 2:57 PM
Formatted: Font:Italic, Subscript

Daniel K. Riskin 5/7/08 2:58 PM
Formatted: Subscript

Daniel K. Riskin 5/7/08 2:58 PM
Formatted: Font:Not Italic

Daniel K. Riskin 5/7/08 2:59 PM
Formatted: Font:Italic

Daniel K. Riskin 5/7/08 2:59 PM
Formatted: Font:Italic, Subscript

Daniel K. Riskin 5/7/08 2:59 PM
Formatted: Superscript

Daniel K. Riskin 5/7/08 2:59 PM
Formatted: Font:Italic

Daniel K. Riskin 5/7/08 2:59 PM
Formatted: Font:Italic

Daniel K. Riskin 5/7/08 2:59 PM
Formatted: Font:Italic, Subscript

Daniel K. Riskin 5/7/08 2:58 PM
Formatted: Superscript

Daniel K. Riskin 5/7/08 2:58 PM
Formatted: Font:Italic

Daniel K. Riskin 5/7/08 3:00 PM
Formatted: Font:Not Italic

Daniel K. Riskin 5/7/08 3:00 PM
Formatted: Font:Not Italic

304 *3.1 Wingbeat kinematics*

305 Flight speeds of *C. brachyotis* in the wind tunnel ranged from 3.2 to 7.4 $m \cdot s^{-1}$.
306 Wingbeat frequencies (9.4 ± 0.6 Hz, mean ± S.D.) were similar to those reported
307 previously for other bat species flying in still air (Norberg, 1976a), and increased slightly
308 with increased flight speed (frequency = 0.33 × speed + 7.8; $F = 15.9$; $n = 9$; $r^2 = 0.69$; P
309 = 0.0053). In slow flight, the downstroke brought the wing anteriorly and ventrally
310 (forward and down), and the upstroke moved it posteriorly and dorsally (backwards and
311 up). Low speed flight kinematics also included a wingtip reversal on the upstroke,
312 whereby the wingtip (*h* in Figure 1) moved backwards relative to the air around it. At
313 higher speeds, the fore-aft component of that motion was diminished, so the wings
314 moved mostly dorsoventrally (up and down), and without wingtip reversal. These
315 kinematic descriptions resemble those reported for other bats in previous studies
316 (Aldridge, 1986).
317
318 *3.2 Proper Orthogonal Decomposition*

319 Each mode resulting from Proper Orthogonal Decomposition of marker positions
320 describes a range of motion of the markers in 3-dimensional space. A convenient way to
321 visualize the range of motion captured by any given mode is to project the original
322 motion of the markers onto the subspace defined by that mode (e.g. Bozkurttas *et al.*,
323 2006). When a linear coordinate system is used, the positions of each marker in a POD
324 mode lie on a straight line (Figure 2). In this study, projection of the wing kinematics
325 onto the first mode of POD resulted in a simple flapping motion of the wings. For slow
326 flights, the wings moved up and down with a fore-aft component relative to the body

axis, and in faster flights the motion contained less fore-aft motion, and was restricted to up-down movement. These trends mirror the decrease in the fore-aft component of wing flapping with increasing speed that we observed from the kinematics.

From POD of marker positions, the first mode described 31.4 ± 2.8% (n = 9) of kinematic movement, and the amount of variation explained by subsequent modes decreased rapidly (Figure 3a). For any trial, 7 modes were required to explain >80% of the motion, 11 modes were needed to explain >90% of the motion, and 16 of the total 46 orthogonal modes were needed to explain >95% of the motion. The mean $\xi_{95\%}$ value for the 9 trials was 13.5 ± 1.2. Using joint angles instead of marker positions, 22.4 ± 1.8% of motion was explained by the first mode, and the mean $\xi_{95\%}$ value was 13.1 ± 0.8 (Figure 3b).

We found no influence of the number of wingbeats included on $P_{\xi 1}$ (linear regression P = 0.89). However, $\xi_{95\%}$ values did increase slightly with the number of wingbeats in a trial ($\xi_{95\%}$ = 1.57 × number of wingbeats + 8.60; r^2 = 0.58; P = 0.02). Depending on whether one uses $P_{\xi 1}$ or $\xi_{95\%}$ to measure complexity, the number of wingbeats in each trial may or may not need to be equal in all trials for them to be compared. To equilibrate the number of wingbeats for all trials, while losing the least possible information, one could discard a wingbeat from both of the four-wingbeat trials, and the two-wingbeat trial altogether. When we employed this procedure, the regressions of $P_{\xi 1}$ and $\xi_{95\%}$ with speed showed the same statistical trends obtained with the complete data set (reported below). We therefore elected to treat all trials equally in our analyses, and did not weight them based on the number of wingbeats.

3.3: Changes in dimensional complexity with speed

Dimensional complexity varied little among trials, and did not change significantly with speed. For the marker position data, flight speed had no significant impact on $\xi_{95\%}$ values ($\xi_{95\%}$ = -0.16 × speed + 14.28; r^2 = 0.04; P = 0.61). Using joint angle data, $\xi_{95\%}$ values increased slightly with increasing speed ($\xi_{95\%}$ = 0.30 × speed + 11.62; r^2 = 0.32), but not significantly so (P = 0.11).

Daniel K. Riskin 5/7/08 2:23 PM
Deleted: between

3.4: Testing the efficacies of kinematic marker positions

For each of the 32,767 possible combinations of 1 to 15 wing markers (3 to 17 body markers), we calculated $P_{\xi l}$ for all nine trials, and used the mean $P_{\xi l}$ value for each marker combination for analyses (n = 9 trials; Figure 4).

As expected, using more markers generally resulted in higher dimensional complexity overall (lower median $P_{\xi l}$ values), but for a given number of wing markers, the positions of those markers influenced the capture of actual dimensional complexity. Indeed, there are many ways to increase the number of markers without improving the capture of dimensional complexity at all, as evidenced by the overlapping $\xi_{95\%}$ and $P_{\xi l}$-values in Figure 4. Since it is beneficial for researchers to know the performance of each marker combination tested, we provide that information, averaged for all nine trials as supplemental information to this paper (Appendix 1), and present the marker sets with lowest $P_{\xi l}$ values in Figure 5. The marker positions used in other selected studies of bat kinematics are shown as red circles in Figure 4 for comparison.

Daniel K. Riskin 5/11/08 4:45 PM
Deleted: and

Markers at the shoulder and hip (*c* and *o* in Figure 1, respectively) contributed substantially to the dimensional complexity of kinematics (Figure 5a). One possible

373 explanation for this pattern is that more muscle is interposed between the skin and
374 underlying skeleton at the shoulder and hip compared to other anatomical markers,
375 potentially leading to increased skin motion artifact. Therefore, we also present optimal
376 marker sets from those POD analyses that excluded the shoulder and hip (Figure 5b).
377 Our analysis demonstrates that the knee moves independently relative to forelimb
378 markers, and that the 5th digit contributes relatively little motion that is independent of
379 other parts of the wing. These trends are revealed by the consistent appearance of those
380 anatomical markers in the sets of lowest $P_{\xi I}$ values for a given number of markers. We
381 observe these trends whether the shoulder and hip are included or excluded during
382 analysis.
383
384 *3.5: Assignment of joint angle groups*
385 Correlations of motion (mean $P_{\xi I}$ values) among the 190 joint angle pairs varied,
386 with a left-skewed distribution (min 51.1%, max 83.2%, median 59.3%). Using a
387 similarity threshold of 0.7, we found three groups of joint angles based on the cluster
388 analysis (Figure 6). The first group (joint angles 3, 6, 7, 11, and 12) includes the angles
389 between digit V and its neighbouring long bones (the forearm and digit IV), along with
390 the metacarpophalangeal angles of digits III and IV, and rotation of the humerus. The
391 second group (joint angles 4, 8, 9, and 10) includes the carpometacarpal angle of digits
392 III, IV, and V, along with the elbow angle. The third group (joint angles 1, 2, 17, 19, and
393 20) includes the elevation/depression (dorsoventral) and protraction/retraction
394 (craniocaudal) of the humerus, the elevation/depression of the femur, femoral rotation,
395 and the knee angle. By plotting the changes in each joint angle over the course of a

representative trial (scaled to equalize standard deviation), the similarity of joint angles within each of the three groups is immediately visible (Figure 7).

4. Discussion

By delineating the wing kinematics of a flying bat in terms of quantitative dimensional complexity, we processed complex motion to uncover three functional groups of joint angles that should be useful in a broad variety of contexts, including morphology, aerodynamics, and neurobiology. Each group consists of joint angles that move in highly correlated ways during steady flight, and provides a starting point to discern functional units of aeromechanic or neuromuscular relevance for bat flight. For example, these may reflect muscle synergies, analogous to those described in other systems (Tresch *et al.*, 2006). Where accurate kinematic reconstruction is the goal, our results demonstrate that in addition to the commonly used kinematic markers on the wing, the hindlimb should be tracked, and that several parts of digits III and IV must be tracked independently. Also, we found that the bat changed the complexity of motion only slightly with changes in speed, even though the motions of the wings changed in a way that resulted in different flight speeds.

Daniel K. Riskin 5/7/08 3:51 PM
Formatted: Font:Italic

4.1 Quantification of dimensional complexity

To completely describe the motions of 17 independent markers on a flying bat in a body-referenced linear coordinate system requires 46 variables. Using POD, 95% of that motion was described by no more than 16 modes, roughly one third the total number of variables. Using joint angles, capture of 95% of motion required 15 modes, almost

three quarters of the 20 joint angle variables. So how 'complex' is bat flight? Can the dimensional complexity of bat flight be empirically quantified?

We emphasize that the overall trends exhibited by changes in $\xi_{95\%}$ and $P_{\xi l}$ are more meaningful than the numerical values themselves, because there is no empirical scale against which to compare these numerical values to the dimensional complexity of other systems. Within this system, $P_{\xi l}$ varies substantially according to the anatomical locations of markers. Numerical results from future studies on bats could be compared with our results if markers in those studies were placed in the same locations, and this anatomical specificity prohibits numerical comparison of bat flight kinematic complexity with the complexity of locomotion in organisms with different limb structure. Our methods are most useful where changes in complexity are to be analyzed within a single system.

The arbitrary nature of the numerical values obtained by our methods is further evidenced by additional analyses of our data, not presented here, which demonstrated that $\xi_{95\%}$ and $P_{\xi l}$ are influenced by input choices such as whether a body-referenced or global-referenced coordinate system is used, whether a linear or spherical coordinate system is used, or whether or not variances of different marker motions are standardized before singular value decomposition. Adjusting these user inputs on our data resulted in similar trends from POD – such as independence of complexity and speed, and anatomical marker motions at the shoulder and hip that were independent of other marker motions. However, numerical values varied substantially depending on how the data were treated. For example, we reported a $\xi_{95\%}$ value of 13.5 ± 1.2 for marker positions in the nine trials in this study, but had we not standardized variance before performing POD on the same

data, the outcome would have been 8.7 ± 1.3. We found, however, that when the same procedure was used to compare different marker positions or kinematic trials, the overall trends reported here persisted consistently.

$\xi_{95\%}$ and $P_{\Sigma 1}$ are different characterizations of the cumulative distribution of eigenvalues across the matrices that result from POD of a dataset. For two- or three-dimensional matrices, $\xi_{95\%}$ is somewhat meaningless, but we prefer to use $\xi_{95\%}$ where possible, since that value reflects a greater portion of the distribution than $P_{\Sigma 1}$ does. For small numbers of dimensions, however, $P_{\Sigma 1}$ was used. The use of two different descriptors might be problematic, since some distributions might appear dimensionally complex by one metric and not the other. Overall, however, we expect these two metrics to be inversely correlated across datasets. We calculated these two values for all 32,767 permutations of 1-15 markers, for all 9 trials (total = 294,903), and found the two to be inversely correlated (linear r^2 0.45). These metrics, then, are not interchangeable, since apparent dimensional complexity by one metric cannot be inferred from the other. In this study we have used $\xi_{95\%}$ where possible, and not used the metrics together for any analysis.

4.2 Selection of marker sets for studies of kinematics

4.2.1 Number of anatomical markers to be used

Our results demonstrate, perhaps not surprisingly, that following more markers consistently tends to increase the dimensional complexity of motion captured, so tracking the motions of as many parts of the wing as possible is surely the best possible strategy for kinematic studies. However, the time required to track large numbers of markers is

substantial, especially where markers appear and disappear from view throughout the wingbeat cycle, as they do for the folding wings of bats. And, while this cost of adding more markers increases somewhat linearly, the benefit of more and more markers plateaus. For large numbers of markers (> ca. 9), the improvements in median dimensional complexity values associated with increased numbers of markers is smaller than it is for small numbers of markers (< 4, for example; Figure 4). Importantly, the addition of some markers will improve dimensional complexity more than others will. It is our hope that the information presented here will help researchers choose what parts of the wing should be tracked for their purposes (Appendix 1).

When we compare optimum marker sets as determined by POD to anatomical landmarks used for kinematics research in previous studies, we find that workers have tended to choose marker sets that exhibit intermediate dimensional complexity. Where only two wing markers are used, our $P_{\xi l}$ values range from 32.8% to 47.2%. Lindhe Norberg and Winter (Lindhe Norberg & Winter, 2006) tracked the thumb and wingtip, capturing roughly the midpoint ($P_{\xi l}$ = 40.3%) of the $P_{\xi l}$ values possible using that number of markers. Bullen and McKenzie (Bullen & McKenzie, 2002) also used two markers, the shoulder and wingtip ($P_{\xi l}$ = 33.0%). Although the $P_{\xi l}$ value for the Bullen and McKenzie marker set is close to the optimal 2-marker set we found (shoulder and wrist $P_{\xi l}$ = 32.8%), it should be noted that their analysis was limited to one camera view, and therefore did not capture the kinematic complexity of three-dimensional motion at those anatomical locations.

Aldridge (Aldridge, 1986; Aldridge, 1987a) used five markers: the wrist and the tips of digits II, III, IV and V. We did not track the tip of digit II in this study, but it lies

Daniel K. Riskin 5/11/08 12:07 PM
Deleted: added

Daniel K. Riskin 5/11/08 12:08 PM
Deleted: captured by adding additional

Daniel K. Riskin 5/11/08 12:07 PM
Deleted: 5

Daniel K. Riskin 5/11/08 12:07 PM
Deleted: Also

Daniel K. Riskin 5/10/08 3:13 PM
Deleted: 5.46

Daniel K. Riskin 5/10/08 3:14 PM
Deleted: 7.86

Daniel K. Riskin 5/10/08 3:21 PM
Deleted: half

Daniel K. Riskin 5/10/08 3:17 PM
Deleted: 6.72

Daniel K. Riskin 5/10/08 3:21 PM
Deleted: kinematic complexity

Daniel K. Riskin 5/10/08 3:22 PM
Deleted: 5.48

Daniel K. Riskin 5/10/08 3:25 PM
Deleted: 5.46

very close to the second marker we placed on digit III. The $P_{\xi I}$ value for Aldridge's marker set (replacing our second marker on III for his marker on II) is 41.6%, suggesting relatively low dimensional complexity compared to the complete range of five-marker $P_{\xi I}$ values in this study (27.4% to 45.4%).

Norberg (Norberg, 1976a) tracked six of our markers: elbow, wrist, tip of digits III, IV, and V, and the foot. She also tracked the tip of the tail in that study, but the bats in our study have no tail, so we omit that marker from comparison. The $P_{\xi I}$ value for her marker set (36.4%) is near the middle of the range of possible $P_{\xi I}$ values obtainable from six-marker data sets (27.8% to 45.1%).

The tendency of researchers to chose points of intermediate dimensional complexity suggests that correlations among anatomical marker positions are not intuitively discernable, or that independence of motion is not an important criterion for marker selection in other studies. The marker sets with highest dimensional complexity in our study tracked motion of digits III and IV independently, and at more than one position along each of their lengths. Typical kinematics studies follow only the tips of one, or occasionally both, of these digits (e.g. Aldridge, 1986; Lindhe Norberg & Winter, 2006). It is unclear how this reduction of dimensional complexity has affected our understanding of bat flight aerodynamics or energetics, but based on our results, we advise that future studies on bat wing maneuvers include several markers along each of those digits, where possible. Whether or not tracking multiple parts of the wing is necessary in studies of birds or insects could also be investigated using our methods.

4.2.2 Hindlimbs

Daniel K. Riskin 5/10/08 3:27 PM
Deleted: 2.82

Daniel K. Riskin 5/10/08 3:28 PM
Deleted: 1.83

Daniel K. Riskin 5/10/08 3:29 PM
Deleted: 3.02

Daniel K. Riskin 5/10/08 3:38 PM
Deleted: 2.02

Daniel K. Riskin 5/10/08 3:40 PM
Deleted: 1.55 to 2.51

Daniel K. Riskin 5/10/08 12:05 PM
Deleted:

Effective marker sets also revealed that the hindlimb moves independently of the rest of the wing. The hindlimb is rarely included in kinematic studies, though it may have significant aerodynamic effect because it anchors the caudal wing. Indeed, airplane wings have many of their control mechanisms at the trailing edge of the wing. Bats are unique from birds in the participation of the hindlimb with the flight apparatus, and may therefore employ active control of tension and posture at the trailing edge that is not possible for birds. Also, the hindlimbs are actively used by bats during terrestrial locomotion (Riskin *et al.*, 2005; Riskin & Hermanson, 2005; Riskin *et al.*, 2006), so their musculoskeletal architecture is available for recruitment during flight. Tracking the position of the hindlimb during flight is a first step toward elucidating a possible active role for the hindlimb, and electromyography (EMG) of the hip and hindlimb musculature would further clarify the mechanistic basis for independent motion of the hindlimb from the rest of the wing.

Daniel K. Riskin 5/7/08 3:57 PM
Deleted: its

4.2.3 Hip and shoulder

A consistent trend in our data was that when the shoulder or hip was included in POD of a marker subset, the kinematic complexity was high. In other words, movements of the hip and shoulder joints are more weakly correlated to the motions of other wing markers than wing marker motions are to one another. We speculated that one possible source of their independence of motion from the other parts of the wing could be skin motion artifacts, since those markers were separated from the underlying joints by relatively thick layers of muscle compared with other wing markers. However, that independence might also have resulted from the three-dimensional skeletal morphology

Daniel K. Riskin 5/11/08 9:01 AM
Deleted: Our analyses suggest a distinctive charac

Daniel K. Riskin 5/11/08 8:52 AM
Deleted: ter of

Daniel K. Riskin 5/11/08 8:59 AM
Deleted: motion

Daniel K. Riskin 5/11/08 8:59 AM
Deleted: at both

of those joints; each ball-and-socket joint has three degrees of freedom of motion, while the majority of the more distal wing joints each bend more or less along one axis, controlled by a smaller, simpler set of muscles, in some cases reduced to a single flexor and extensor pair (Humphry, 1869; Macalister, 1872; Vaughan, 1959). Indeed, the shoulder is controlled by a complex suite of muscles, and experimental studies have demonstrated unique patterns of activation in each of 17 different shoulder muscles (Hermanson & Altenbach, 1983; Hermanson & Altenbach, 1985). A similarly large number of muscles cross the hip (Humphry, 1869; Macalister, 1872), but their patterns of activation are not known. The relative influences of skin motion artifacts and actual kinematic independence on the observed kinematic complexity of motion will soon be quantifiable, thanks to emerging three-dimensional cineradiography techniques (Brainerd *et al.*, 2007).

Daniel K. Riskin 5/7/08 3:58 PM
Deleted: have not been recorded

4.2.4 How much complexity is needed?

Without sufficiently reproducing the dimensional complexity of flight, models will be unable to accurately explain the aeromechanics of actual organisms. What level of fidelity is necessary, however, is not known. Many current models of bat flight treat airflow over the wings as laminar and steady (Norberg, 1987; Norberg & Rayner, 1987; Rayner, 1999), but recent particle image velocimetry results from flying bats point to a wake pattern that varies in complicated ways both spatially and temporally (Hedenström *et al.*, 2007; Tian *et al.*, 2006). Also, leading edge vortices (LEVs), once thought to be irrelevant to flapping flight have recently been detected for flying bats (Muijres *et al.*, 2008), suggesting that the aerodynamics of flight are far more complex than once

Daniel K. Riskin 5/11/08 9:03 AM
Deleted: accurately

Daniel K. Riskin 5/11/08 9:03 AM
Deleted: reproducing the

Daniel K. Riskin 5/11/08 9:11 AM
Deleted: of animal flight are unlikely

Daniel K. Riskin 5/7/08 6:01 PM
Deleted: above the scale of insects, have been detected in flapping physical models well above the size range of most bats

Daniel K. Riskin 5/7/08 6:09 PM
Formatted: Font:Italic

Daniel K. Riskin 5/7/08 6:01 PM
Deleted: (Hubel & Tropea, 2007)

Daniel K. Riskin 5/7/08 6:09 PM
Deleted: LEVs may play a role in bat flight as well

believed. To accurately determine the precise mechanisms of lift and thrust production, models of the wing motions of bats should be reproduced faithfully, conserving as much complexity as possible. Bozkurttas et al. (2006) have demonstrated that for the reconstruction of fish pectoral fin movements, three POD modes (67% of the original motion) produce 92% of the thrust that results from the original motion. Their analysis, however, included 300 kinematic markers on a single fin. For bat flight, a small number of POD modes might also be sufficient, but the efficacy of a reduced-dimension model may well be compromised by omission of certain parts of the wing.

In the future, we can look forward to understanding what parts of the wing are most relevant to a particular line of investigation, so that only a small number of kinematic markers is necessary, but until the mechanisms of aerodynamic force generation in bats are better understood, or until the contribution of each muscle involved in flight control is uncovered, one should follow as much of the wing as one can. Our results on the interdependence of marker motions are useful guides to selecting limited marker sets, where the goal is to maximise kinematic information per marker, especially in the absence of robustly supported hypotheses about which parts of the body are of greatest functional importance.

Our study is limited to a single individual of a single species, so the optimal marker sets we discuss might well not be optimal for other bats. In general, the flight kinematics in *C. brachyotis* are similar to those reported for other bat species, so our suggested marker sets are likely helpful regardless of species, but as fine-scale kinematics studies reveal kinematic differences among species, species-specific optimal marker sets can be prescribed using our method.

Finally, the 17-marker configuration we employed in this analysis did not include markers on the free membrane, where kinematics are sure to have important aerodynamic effects, especially at the leading edge and trailing edge of the wing. The motion of the membranes can not simply be interpolated based on the bone positions. The skin exhibits non-linear elasticity and anisotropy (Swartz *et al.*, 1996), so even a uniform aerodynamic force could produce a variable billowing of the wing membrane that depends on local mechanical properties, the degree to which it is already strained, and on the influence of the plagiopatagiales muscles within the membrane itself (Holbrook & Odland, 1978). Future work based on an even larger marker set may shed more light on the actual complexity of bat motion beyond what is captured by our 17-marker set.

4.3 Functional groups of joints in the flight apparatus of bats

Several papers concerning the aerodynamics of flight in bats treat wings as non-flapping extensions of the body, with a fixed shape that can be described in two dimensions (Norberg, 1987; Norberg & Rayner, 1987). However, the actual shapes of wings change in three dimensions throughout a wingbeat cycle, and we have shown that wing kinematics require around 15 independent dimensions to be described with 95% accuracy. This leaves researchers wishing to use bat wing kinematics for modeling purposes to choose between almost certainly over-simplified models on the one hand, or characterizations of bat flight that may be too complex for functional relationships to be resolved. We present three groups of joints that are of particular value for characterizing bat wing motions using a relatively small number of dimensions. In studies where researchers wish to know the influence of some independent variable on flight

603 kinematics, we suggest using one representative joint angle from each group as a starting
604 point, since those three joints would then give information about 14 of the 20 joints
605 angles that we measured.

606 There are several possible reasons that that joint angles change together in groups.
607 First, actuation of multiple joints may be controlled together; a muscle-tendon 'group'
608 may cross more than one joint, or groups of muscles may be innervated by a single motor
609 pool from the nervous system (Burke, 1978; Goslow, 1985). Either mechanism could
610 lead to patterns of correlated joint motion. Second, the motions of some joints influence
611 motion at other joints because the wing membrane is a single continuous structure; full
612 extension of a single digit, for example, might not be possible if the neighbouring digits
613 are folded. Third, different parts of the wing surely need to move together for changes at
614 any one of them to effectively generate aerodynamic force, or for fluid structures along
615 the wing, such as LEVs, to be maintained. In this scenario, effective flight performance
616 may require portions of the wing with neuromuscular and structural independence to
617 move in strict relation to one another. These three explanations are in no way exclusive,
618 and any or all of these explanations may underlie the existence of highly correlated
619 clusters of joint angles.

620 Alternatively, it is possible that these functional groups emerged by chance – that
621 there is a random distribution of correlations among the joints, and we simply picked the
622 most tightly correlated – but this is unlikely. Had this been the case, we would expect the
623 members of a group to be distributed somewhat randomly across the wing. Instead, we
624 find that our groups occur close to one another anatomically. We therefore consider these

Daniel K. Riskin 5/7/08 9:39 PM
Deleted: if present,

625 groups good candidate functional units for models intended to simplify the complex
626 kinematics of bat flight.
627 A simplified way to report our results from analysis of temporal correlation
628 among joints to specify three coherent joint assemblages: (1) wing spreading and finger-
629 bending (2) angle of the wrist relative to body pitch and elbow bending, and (3) actuation
630 of the medial portion of the wing by the shoulder, hip, and knee. A simplified model that
631 moved the joints within a group as a unit might have just one degree of freedom per
632 group, but describe a great deal of motion present in an actual bat wing during flight.
633 The composition of joint angles in the first group demonstrates that the fingers are
634 not spread in unison during flight; the angle between digits III and IV changes with
635 different timing from the spread among digits IV, V, and the forearm. Similarly, bending
636 at the mid-digital (metacarpophalangeal) joint does not occur in synchrony among all
637 digits. While metacarpophalangeal bending of joints III and IV is tightly coupled, this
638 pair moves independently of metacarpophalangeal joint V. This might facilitate bulk
639 movement of air along the surface of the wing during a wingbeat cycle.
640 That the three carpometacarpal angles in group two move together simply means
641 that metacarpophalangeal flexion/extension occurs in synchrony for digits III, IV, and V
642 – that the membrane between them forms a flat surface hinged at the wrist. In this sense,
643 modeling the portion of the wing closest to the wrist as a simple flapping plate may be
644 appropriate for many kinds of studies. Interestingly, this ‘plate’ moves in synchrony with
645 elbow angle.
646 The third group consists of motion of the wing at the regions where it attaches to
647 the body. This includes motion at the humerus (craniocaudal and dorsoventral motion),

and the hip (craniocaudal, dorsoventral, and rotational movements). This group of joints is more likely to move together for aerodynamic reasons than for musculoskeletal ones, since the branches of the CNS innervating the fore and hindlimbs are distinct. Air flow over the proximal wing likely requires correlated motions at the leading and trailing edges of the wing.

4.4 Predictions and future validation

If the three synchronously moving groups we have described result from neuroanatomical compartmentalization of the flight apparatus, this might be further elucidated by detailed EMG of the flight muscles, building on the work on shoulder muscle activity in bats during flight done by Hermanson and Altenbach (Hermanson & Altenbach, 1983; Hermanson & Altenbach, 1985). Detailed anatomical description of *C. brachyotis* would be necessary as a first step though, since the attachment of intrinsic wing and hindlimb muscles can vary substantially among species, and have not been described for our focal species. Predictions from our data of how muscle activation timing should occur are further complicated by the fact that we do not know the spatial or temporal distribution of aerodynamic forces along the wing. Like ground reaction forces in terrestrial locomotion (Roberts & Belliveau, 2005; Schmidt, 2006), these would have considerable influence on the timing of muscle activation.

For modeling purposes, we recommend these groups of joints as candidates for models of neuromuscular and aerodynamic control, and for modeling of bat flight where the actual kinematics possess too many variables for the model in question. Our three joint groups provide an intermediate between the stiff, non-flapping wing that has been

used for modeling previously, and the highly complicated wing kinematics of bats that make modeling so difficult. Validation of the utility of our three functional units for studies of aerodynamics could be achieved through a computational fluid dynamic models such as FastAero, of the kind described by Willis et al. (Willis *et al.*, 2007), comparing fully reconstructed wake patterns from full kinematic reconstruction to the aerodynamics inferred based on simplified models that use our three groups.

Our analysis of dimensional complexity has uncovered information useful for the capture and analysis of kinematic data involving bats, and has uncovered three functional groups upon which neurobiological and aeromechanic studies can be based. We have demonstrated that bat flight, though very complex, can be simplified in a meaningful way. Our methods should also be applicable to other kinematic studies, where simplified models are desired.

5. Acknowledgments

We are deeply appreciative of a large team of staff, undergraduate, graduate, and postdoctoral workers at Brown University who 'clicked' the ca. 200,000 points digitized for this project. We also thank Igor Pivkin for some early work on methods of POD output visualization, Kevin M. Middleton for assistance with statistical analyses, and Ben Dickinson, Gregory Shakhnarovich, and five anonymous reviewers for helpful comments on earlier versions of this manuscript. Andrew A. Biewener, staff, and students at the Concord Field Station of Harvard University provided housing and care for our animals, granted us use of their wind tunnel, and engaged us in many helpful conversations about this work. This study was supported by the United States Air Force Office of Scientific

694 Research (AFOSR) monitored by R. Jefferies and W. Larkin, the National Science
695 Foundation (NSF), and the Brown University Undergraduate Teaching and Research
696 Awards (UTRA) Program.

697

Daniel K. Riskin 5/10/08 12:09 PM
Formatted: Indent: First line: 0"

698 **6. References**

699 Aldridge, H. D. J. N. (1986). Kinematics and aerodynamics of the greater horseshoe bat,
700 *Rhinolophus ferrumequinum*, in horizontal flight at various flight speeds. *Journal*
701 *of Experimental Biology* **126**, 479-497.
702 Aldridge, H. D. J. N. (1987a). Body accelerations during the wingbeat in six bat species:
703 the function of the upstroke in thrust generation. *Journal of Experimental Biology*
704 **130**, 275-293.
705 Aldridge, H. D. J. N. (1987b). Turning Flight of Bats. *Journal of Experimental Biology*
706 **128**, 419-425.
707 Bozkurttas, M., Dong, H., Mittal, R., Madden, P. & Lauder, G. V. (2006). *American*
708 *Institute of Aeronautics and Astronautics Aerospace Sciences Meeting and*
709 *Exhibit, Reno, NV*.
710 Brainerd, E. L., Gatesy, S. M., Baier, D. B. & Hedrick, T. L. (2007). *International*
711 *Congress for Vertebrate Morphology 8, Paris*.
712 Bullen, R. D. & McKenzie, N. L. (2002). Scaling bat wingbeat frequency and amplitude.
713 *Journal of Experimental Biology* **205**, 2615-2626.
714 Burke, R. E. (1978). Motor units: physiological/histochemical profiles, neural
715 connectivity and functional specializations. *American Zoologist* **18**, 127-134.

716 Cappellini, G., Ivanenko, Y. P., Poppele, R. E. & Lacquaniti, F. (2006). Motor Patterns in
717 Human Walking and Running. *Journal of Neurophysiology* **95**(6), 3426-3437.
718 Chatterjee, A. (2000). An introduction to proper orthogonal decomposition. *Current*
719 *Science* **78**(7), 808-817.
720 Chau, T. (2001). A review of analytical techniques for gait data. Part 1: fuzzy, statistical
721 and fractal methods. *Gait & Posture* **13**(1), 49-66.
722 Daffertshofer, A., Lamoth, C. J. C., Meijer, O. G. & Beek, P. J. (2004). PCA in studying
723 coordination and variability: a tutorial. *Clinical Biomechanics* **19**, 415-428.
724 Feeny, B. F. & Kappagantu, R. (1998). On the physical interpretation of proper
725 orthogonal modes in vibrations. *Journal of Sound and Vibration* **211**(4), 607-616.
726 Forner-Cordero, A., Levin, O., Li, Y. & Swinnen, S. P. (2007). Posture control and
727 complex arm coordination: Analysis of multijoint coordinate movements and
728 stability of stance. *Journal of Motor Behavior* **39**(3), 215-226.
729 Goslow, G. E. (1985). Neural control of locomotion. In *Functional vertebrate*
730 *morphology* (Hildebrand, M., Bramble, D. M., Liem, K. F. & Wake, D. B., eds.),
731 pp. 338-365. Belknap Press of Harvard University Press, Cambridge, Mass.
732 Hedenström, A., Johansson, L. C., Wolf, M., von Busse, R., Winter, Y. & Spedding, G.
733 R. (2007). Bat flight generates complex aerodynamic tracks. *Science* **316**, 894-
734 897.
735 Hedrick, T. L., Tobalske, B. W. & Biewener, A. A. (2002). Estimates of circulation and
736 gait change based on a three-dimensional kinematic analysis of flight in cockatiels
737 (*Nymphicus hollandicus*) and ringed turtle-doves (*Streptopelia risoria*). *Journal of*
738 *Experimental Biology* **205**(10), 1389-1409.

739 Hedrick, T. L., Usherwood, J. R. & Biewener, A. A. (2004). Wing inertia and whole-
740 body acceleration: an analysis of instantaneous aerodynamic force production in
741 cockatiels (*Nymphicus hollandicus*) flying across a range of speeds. *Journal of*
742 *Experimental Biology* **207**(10), 1689-1702.
743 Hermanson, J. W. & Altenbach, J. S. (1983). The functional anatomy of the shoulder of
744 the Pallid Bat, *Antrozous pallidus*. *Journal of Mammalogy* **64**(1), 62-75.
745 Hermanson, J. W. & Altenbach, J. S. (1985). Functional anatomy of the shoulder and arm
746 of the fruit-eating bat *Artibeus jamaicensis*. *Journal of Zoology* **205**, 157-177.
747 Holbrook, K. A. & Odland, G. F. (1978). A collagen and elastic network in the wing of a
748 bat. *Journal of Anatomy* **126**(1), 21-36.
749 Hotelling, H. (1933). Analysis of a complex of statistical variables into principle
750 components. *Journal of Educational Psychology* **24**(6), 417-441.
751 Humphry, G. M. (1869). The myology of the limbs of *Pteropus*. *Journal of Anatomy and*
752 *Physiology* **3**, 294-319.
753 Ivanenko, Y. P., d'Avella, A., Poppele, R. E. & Lacquaniti, F. (2008). On the origin of
754 planar covariation of elevation angles during human locomotion. *Journal of*
755 *Neurophysiology* **99**(4), 1890-1898.
756 Liang, Y. C., Lee, H. P., Lim, S. P., Lin, W. Z., Lee, K. H. & Wu, C. G. (2002). Proper
757 orthogonal decomposition and its applications - Part I: Theory. *Journal of Sound*
758 *and Vibration* **252**(3), 527-544.
759 Lindhe Norberg, U. M., Brooke, A. P. & Trewhella, W. J. (2000). Soaring and non-
760 soaring bats of the family Pteropodidae (fying foxes, *Pteropus* spp.): Wing

761 morphology and flight performance. *Journal of Experimental Biology* **203**(3),
762 651-664.
763 Lindhe Norberg, U. M. & Winter, Y. (2006). Wing beat kinematics of a nectar-feeding
764 bat, *Glossophaga soricina*, flying at different flight speeds and Strouhal numbers.
765 *Journal of Experimental Biology* **209**(19), 3887-3897.
766 Macalister, A. (1872). The myology of the Cheiroptera. *Philosophical Transactions of*
767 *the Royal Society of London* **162**, 125-173.
768 Mason, C. R., Gomez, J. E. & Ebner, T. E. (2001). Hand synergies during reach-to-grasp.
769 *Journal of Neurophysiology* **86**, 2896-2910.
770 Muijres, F. T., Johansson, L. C., Barfield, R., Wolf, M., Spedding, G. R. & Hedenström,
771 A. (2008). Leading-Edge Vortex Improves Lift in Slow-Flying Bats. *Science*
772 **319**(5867), 1250-1253.
773 Norberg, R. A. (1987). Wing form and flight mode in bats. In *Recent advances in the*
774 *study of bats* (Fenton, M. B., Racey, P. A. & Rayner, J. M. V., eds.), pp. 43-56.
775 Cambridge University Press, Cambridge.
776 Norberg, U. M. (1969). An arrangement giving a stiff leading edge to the hand wing in
777 bats. *Journal of Mammalogy* **50**(4), 766-770.
778 Norberg, U. M. (1970). Functional osteology and myology of the wing of *Plecotus*
779 *auritus* Linnaeus (Chiroptera). *Arkiv für Zoologi* **33**(5), 483-543.
780 Norberg, U. M. (1972). Functional osteology and myology of the wing of the dog-faced
781 bat *Rousettus aegyptiacus* (É. Geoffroy) (Mammalia, Chiroptera). *Z. Morph. Tiere*
782 **73**, 1-44.

783 Norberg, U. M. (1976a). Aerodynamics, kinematics and energetics of horizontal flapping
784 flight in the long-eared bat *Plecotus auritus*. *Journal of Experimental Biology* **65**,
785 179-212.
786 Norberg, U. M. (1976b). Some advanced flight manoeuvres of bats. *Journal of*
787 *Experimental Biology* **64**, 489-495.
788 Norberg, U. M. & Rayner, J. M. V. (1987). Ecological morphology and flight in bats
789 (Mammalia, Chiroptera) - wing adaptations, flight performance, foraging strategy
790 and echolocation. *Philosophical Transactions of the Royal Society of London B*
791 *Biological Sciences* **316**(1179), 337-419.
792 Pearson, K. (1901). On lines and planes of closest fit to systems of points in space.
793 *Philosophical Magazine* **2**, 559-572.
794 Rayner, J. M. V. (1999). Estimating power curves of flying vertebrates. *Journal of*
795 *Experimental Biology* **202**(23), 3449-3461.
796 Rayner, J. M. V. & Aldridge, H. D. J. N. (1985). Three-dimensional reconstruction of
797 animal flight paths and the turning flight of microchiropteran bats. *Journal of*
798 *Experimental Biology* **118**(1), 247-265.
799 Riskin, D. K., Bertram, J. E. A. & Hermanson, J. W. (2005). Testing the hindlimb-
800 strength hypothesis: Non-aerial locomotion by Chiroptera is not constrained by
801 the dimensions of the femur or tibia. *Journal of Experimental Biology* **208**(7),
802 1309-1319.
803 Riskin, D. K. & Hermanson, J. W. (2005). Independent evolution of running in vampire
804 bats. *Nature* **434**(7031), 292.

805 Riskin, D. K., Parsons, S., Schutt, W. A., Jr., Carter, G. G. & Hermanson, J. W. (2006).
806 Terrestrial locomotion of the New Zealand Short-tailed Bat *Mystacina*
807 *tuberculata* and the Common Vampire Bat *Desmodus rotundus*. *Journal of*
808 *Experimental Biology* **209**(9), 1725-1736.
809 Roberts, T. J. & Belliveau, R. A. (2005). Sources of mechanical power for uphill running
810 in humans. *Journal of Experimental Biology* **208**(10), 1963-1970.
811 Rosen, M., Spedding, G. R. & Hedenström, A. (2004). The relationship between
812 wingbeat kinematics and vortex wake of a thrush nightingale. *Journal of*
813 *Experimental Biology* **207**(24), 4255-4268.
814 Schmidt, M. (2006). Quadrupedal locomotion in squirrel monkeys (Cebidae: *Saimiri*
815 *sciureus*): A cineradiographic study of limb kinematics and related substrate
816 reaction forces. *American Journal of Physical Anthropology* **128**, 359-370.
817 Spedding, G. R. (1987). The wake of a kestrel (*Falco tinnunculus*) in flapping flight.
818 *Journal of Experimental Biology* **127**(1), 59-78.
819 Spedding, G. R., Rayner, J. M. V. & Pennycuick, C. J. (1984). Momentum and energy in
820 the wake of a pigeon (*Columba livia*) in slow flight. *Journal of Experimental*
821 *Biology* **111**(1), 81-102.
822 Spedding, G. R., Rosén, M. & Hedenström, A. (2003). A family of vortex wakes
823 generated by a thrush nightingale in free flight in a wind tunnel over its entire
824 natural range of flight speeds. *Journal of Experimental Biology* **206**, 2313-2344.
825 Swartz, S. M., Bennett, M. B. & Carrier, D. R. (1992). Wing bone stresses in free flying
826 bats and the evolution of skeletal design for flight. *Nature* **359**(6397), 726-729.

827 Swartz, S. M., Groves, M. S., Kim, H. D. & Walsh, W. R. (1996). Mechanical properties
828 of bat wing membrane skin. *Journal of Zoology* **239**, 357-378.
829 Tangorra, J. L., Davidson, S. N., Hunter, I. W., Madden, P. G. A., Lauder, G. V., Dong,
830 H., Bozkurttas, M. & Mittal, R. (2007). The development of a biologically
831 inspired propulsor for unmanned underwater vehicles. *IEEE Journal of Oceanic*
832 *Engineering* **32**(3), 533-550.
833 Tian, X., Iriarte-Diaz, J., Middleton, K. M., Galvao, R., Israeli, E., Roemer, A., Sullivan,
834 A., Song, A., Swartz, S. M. & Breuer, K. S. (2006). Direct measurements of the
835 kinematics and dynamics of bat flight. *Bioinspiration and Biomimetics* **1**, S10-
836 S18.
837 Todorov, E. & Ghahramani, Z. (2004). *Engineering in Medicine and Biology Society,*
838 *2004. IEMBS '04. 26th Annual International Conference of the IEEE*.
839 Tresch, M. C., Cheung, V. C. K. & d'Avella, A. (2006). Matrix Factorization Algorithms
840 for the Identification of Muscle Synergies: Evaluation on Simulated and
841 Experimental Data Sets. *Journal of Neurophysiology* **95**(4), 2199-2212.
842 Tripp, B. L., Uhl, T. L., Mattacola, C. G., Srinivasan, C. & Shapiro, R. (2006). A
843 comparison of individual joint contributions to multijoint position reproduction
844 acuity in overhead-throwing athletes. *Clinical Biomechanics* **21**(5), 466-473.
845 Vaughan, T. A. (1959). Functional morphology of three bats: *Eumops*, *Myotis*, *Macrotus*.
846 *University of Kansas Publications Museum of Natural History* **12**(1), 1-153.
847 Watts, P., Mitchell, E. J. & Swartz, S. M. (2001). A computational model for estimating
848 the mechanics of horizontal flapping flight in bats: model description and
849 validation. *Journal of Experimental Biology* **204**, 2873-2898.

Willis, D. J., Kostandov, M., Riskin, D. K., Peraire, J., Laidlaw, D. H., Swartz, S. M. & Breuer, K. S. (2007). Modeling the flight of a bat (Science Magazine Feature).

7. Figure Legends

Figure 1: Image, obtained from one of the high-speed cameras, of *Cynopterus brachyotis* in flight at 3.2 $m \cdot s^{-1}$. We used 17 markers: anterior and posterior sternum (*a* and *b*, respectively), shoulder (*c*), elbow (*d*), wrist (*e*), the metacarpophalangeal and interphalangeal joints and tips of digits III (*f*, *g*, *h*), IV (*i*, *j*, *k*), and V (*l*, *m*, *n*), the hip (*o*), knee (*p*), and foot (*q*).

Figure 2: Ventral view of paths taken by the elbow (light blue), wrist (green), foot (purple), and the tips of digits III (dark blue) and IV (red) for a bat performing three consecutive wingbeats while flying at 4.8 $m \cdot s^{-1}$: (A) The original kinematic data, captured by manually digitizing video images of the bat in flight; (B) The same data, after missing points were filled with a gap-filling algorithm and high-frequency noise was removed with a 50 Hz Butterworth lowpass filter; (C) Mode 1 found by POD of the trial, which contains 34.1% of the kinematic motion present in B; (D) Mode 2, orthogonal to Mode 1, that contains 23.2% of the kinematic data present in B; and (E) the combination of the first two modes, which combined demonstrate 57.3% of the kinematic motion. Note that only the motions of only five points are shown, but that each POD mode describes a range of positions for all kinematic markers.

Figure 3: Percentage of motion described by the m^{th} mode (red dots), and the cumulative total of percent motion described by modes 1 to m (black dots) from POD analysis of the marker motions (A) and joint angles (B). Dots represent mean values for the nine trials, and error bars extend one standard deviation above and below the mean. Complete

kinematic reconstruction is denoted by the dashed black line at 100%. The mean 95% kinematic reconstruction (dashed red line) occurs at $\xi_{95\%} = 13.5$ for marker positions, and 13.1 for joint angles.

Figure 4: Percent recovery by the first POD mode ($P_{\xi 1}$) for the 32,767 different marker combinations possible using both sternum markers and 1 to 15 wing markers. Each black circle represents the mean value for a set of markers ($n = 9$ trials), and each blue bar represents the median $P_{\xi 1}$ value for all marker position permutations with that number of wing markers. Values are distributed on the x-axis according to the number of wing markers in each set. When six wing markers are used, the placement of those markers can result in any of 5,005 $P_{\xi 1}$ values, from relatively poor capture of kinematic complexity (where a single mode recovers 45.1% of the original motion (i), to better capture of dimensional complexity (mode 1 recovers just 27.8%; ii). Wing marker configurations from other studies are shown as red circles: (A) Lindhe Norberg and Winter, 2006; (B) Bullen and McKenzie, 2001; (C) Aldridge, 1986, 1987a; (D) Norberg 1976.

Daniel K. Riskin 5/10/08 3:48 PM
Deleted: ,

Daniel K. Riskin 5/10/08 3:48 PM
Deleted: divided by the number of degrees of freedom in that analysis

Daniel K. Riskin 5/10/08 3:48 PM
Deleted: point

Daniel K. Riskin 5/10/08 3:49 PM
Deleted: marker set in all nine trials

Daniel K. Riskin 5/10/08 3:49 PM
Deleted: used

Daniel K. Riskin 5/10/08 4:55 PM
Deleted: Inset:

Daniel K. Riskin 5/10/08 4:53 PM
Deleted: (18 degrees of freedom)

Daniel K. Riskin 5/10/08 5:15 PM
Deleted: several

Daniel K. Riskin 5/10/08 5:15 PM
Deleted: ,

Daniel K. Riskin 5/10/08 3:51 PM
Deleted: 9

Daniel K. Riskin 5/10/08 5:15 PM
Deleted: %,

Figure 5: (A) For each number of wing markers, 1 to 15, the set of markers that captures the greatest dimensional complexity is shown. Since the shoulder and hip may have moved independently of other markers due to skin motion artifacts, we also show (B) the optimal sets that exclude those points, using 1 to 13 wing markers.

Figure 6: Dendrogram of joint angles, calculated using the average linkage function in Matlab, with (1- $P_{\xi 1}$) values for all 190 joint angle pairs used as the dissimilarity matrix.

The groups are shown in red (group 1), blue (group 2), and green (group 3). Joint angles are defined in Table 1.

Figure 7: Twenty standardized joint angles of a flying bat over time for a single trial, at 4.4 $m \cdot s^{-1}$. Downstrokes are shown in grey. Note that joint angles within each group are tightly correlated. To standardize each joint angle, we have subtracted the mean joint angle over the course of the trial from each value in the time series, then divided each value in the time series by the standard deviation of that joint angle in the trial. Some joint angles (2, 3, and 5) were then multiplied by -1 to facilitate the comparison of their motion with that of other joint angles. Joint angles are defined in Table 1.

910 **Table 1: Joint angles used in this study. Italicized letters denote joint positions, as**
911 **shown in Figure 1.**

joint angle number	definition	calculation
angle 1	humeral elevation/depression (dorsoventral angle)	spherical coordinates of *c-d*, relative to the body-referenced *x*-axis (assumes no body roll)
angle 2	humeral protraction/retraction (craniocaudal angle)	
angle 3	humeral rotation	angle of *a-b* to the plane defined by *c-d-e*
angle 4	elbow flexion/extension	angle *c-d-e*
angle 5	abduction/adduction of digits III & IV	angle *i-e-f*
angle 6	abduction/adduction of digits IV & V	angle *l-e-i*
angle 7	abduction/adduction between digit V & forearm	angle *d-e-l*
angle 8	carpometacarpal flexion/extension of digit III	angle of *e-f* relative to the plane defined by *c-d-e*
angle 9	carpometacarpal flexion/extension of digit IV	angle of *e-i* relative to the plane defined by *c-d-e*
angle 10	carpometacarpal flexion/extension of digit V	angle of *e-l* relative to the plane defined by *c-d-e*
angle 11	metacarpophalangeal flexion/extension of digit III	angle *e-f-g*
angle 12	metacarpophalangeal flexion/extension of digit IV	angle *e-i-j*
angle 13	metacarpophalangeal flexion/extension of digit V	angle *e-l-m*
angle 14	interphalangeal flexion/extension of digit III	angle *f-g-h*
angle 15	interphalangeal flexion/extension of digit IV	angle *i-j-k*
angle 16	interphalangeal flexion/extension of digit V	angle *l-m-n*
angle 17	femoral elevation/depression (dorsoventral angle)	spherical coordinates of *o-p*, relative to the body-referenced *x*-axis (assumes no body roll)
angle 18	femoral abduction/adduction (craniocaudal angle)	
angle 19	femoral rotation	angle of *a-b* relative to the plane defined by *o-p-q*
angle 20	knee flexion/extension	angle *o-p-q*

912

913

Figure 1:

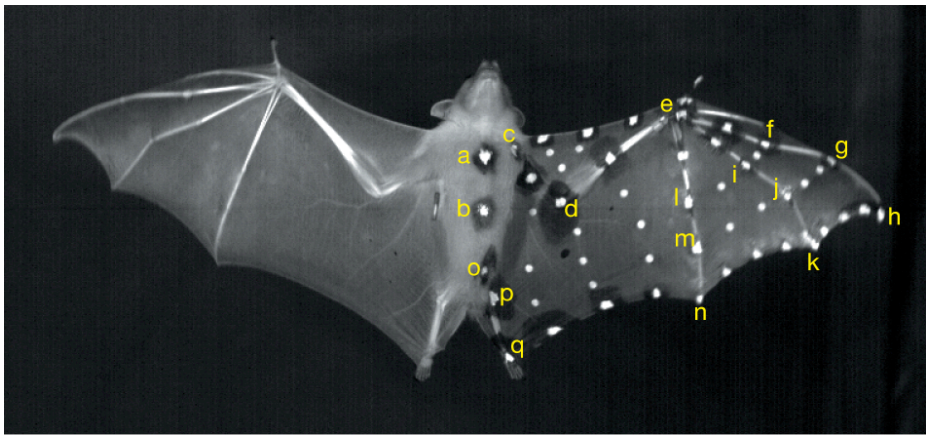

Figure 2:

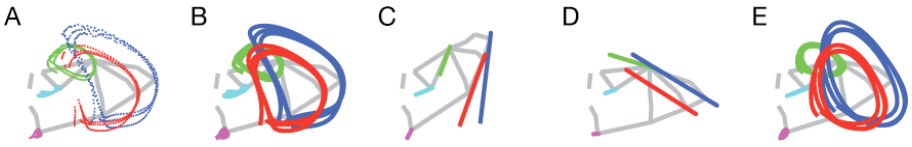

Figure 3:

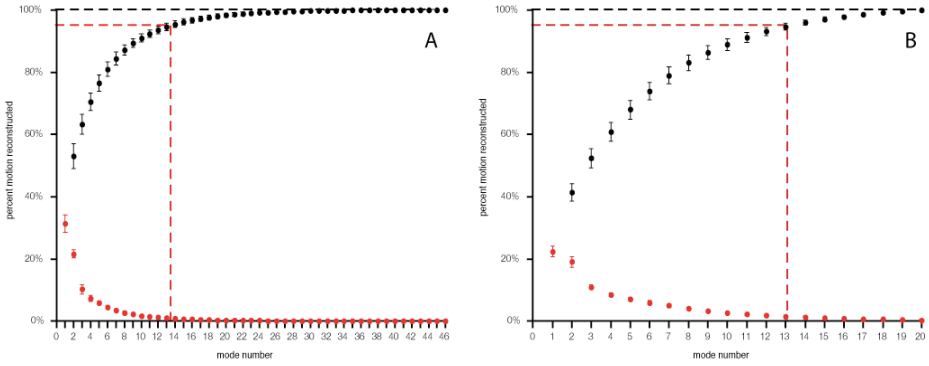

Figure 4:

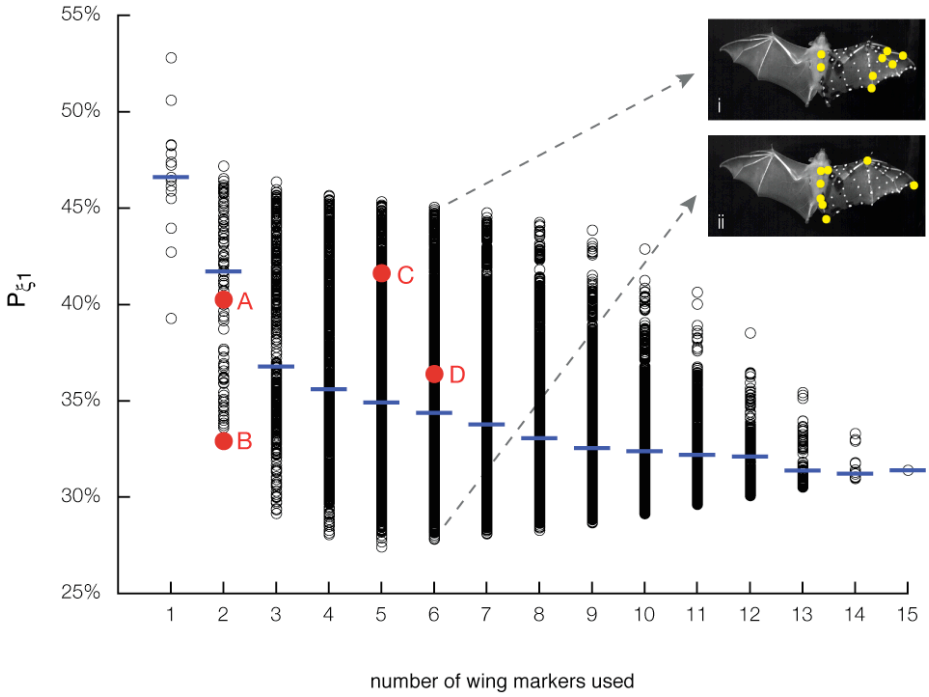

Figure 5:

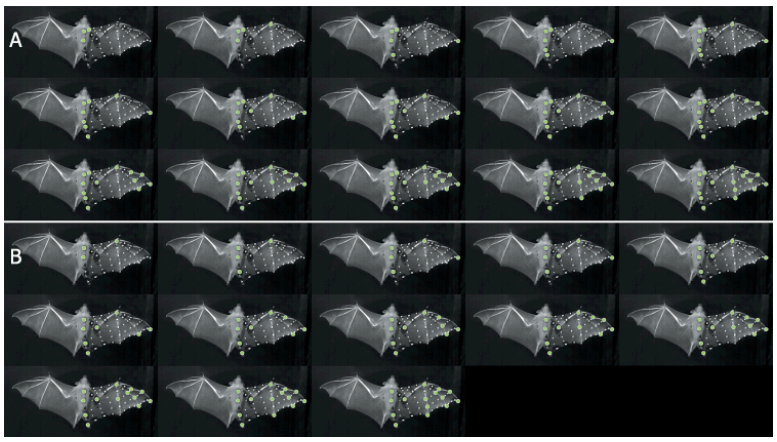

924 **Figure 6:**

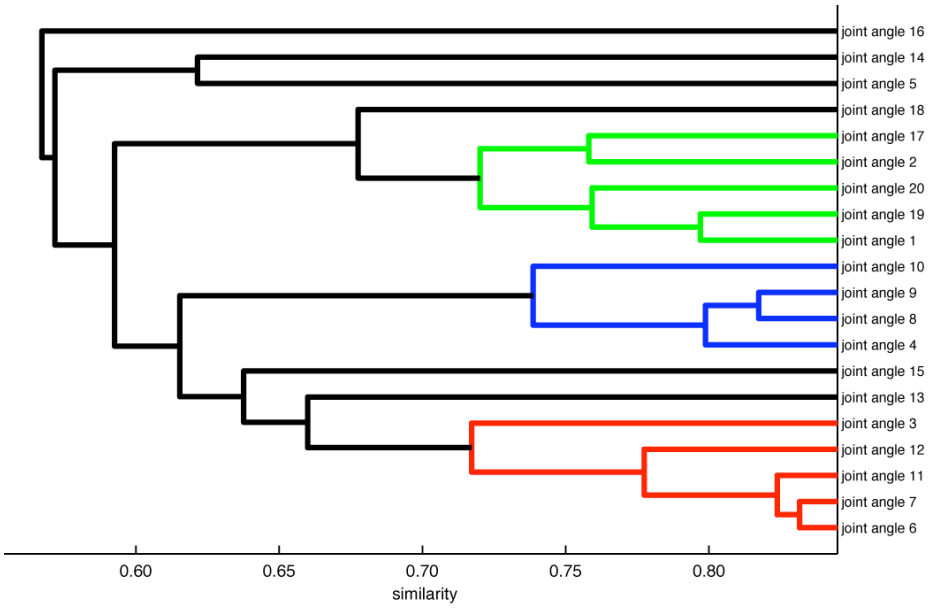

925

926

926 **Figure 7:**

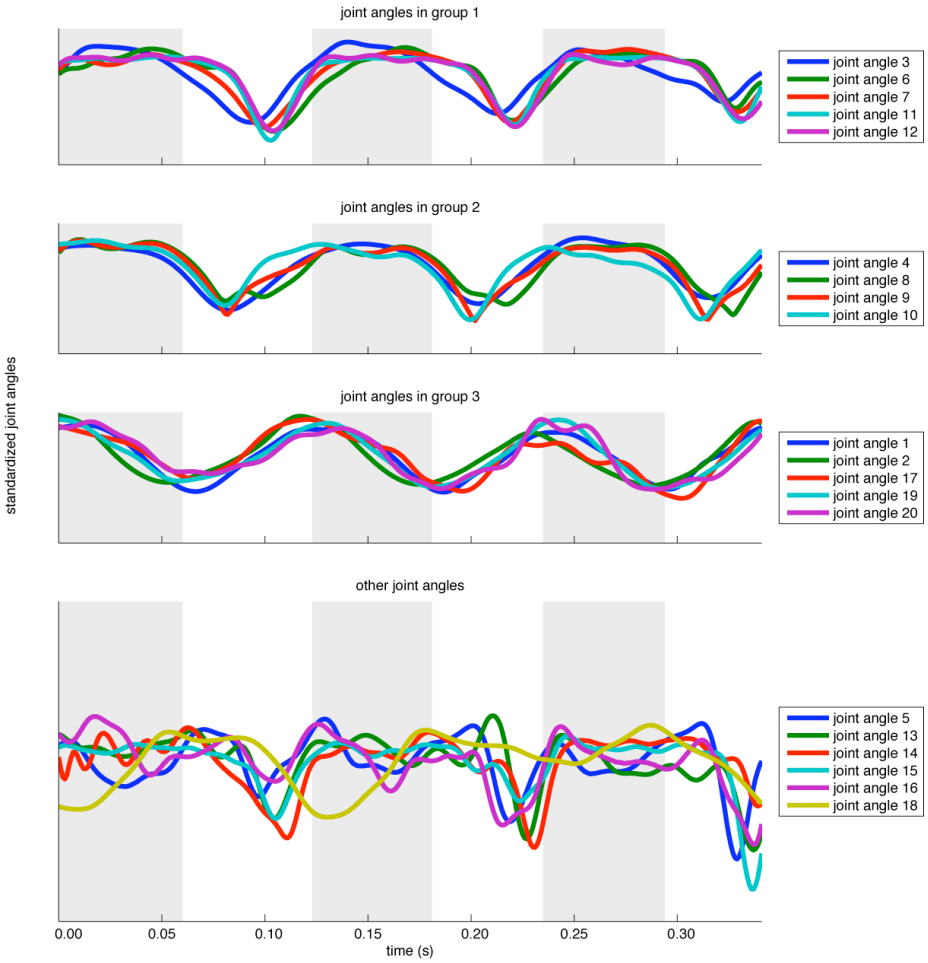

927